J. Fluid Mech. (1992), *vol.* 237, *pp.* 413–434
Printed in Great Britain

Spin-up from rest of a compressible fluid in a rapidly rotating cylinder

By JAE MIN HYUN[1] AND JUN SANG PARK[2]

[1] Department of Mechanical Engineering, Korea Advanced Institute of Science & Technology, P.O. Box 150, Chong Ryang, Seoul, Korea

[2] CAD/CAM, R&D Center, Sam Sung Electro-Mechanics, Suweon, Korea

(Received 13 February 1990 and in revised form 4 October 1991)

Spin-up flows of a compressible gas in a finite, closed cylinder from an initial state of rest are studied. The flow is characterized by small reference Ekman numbers, and the peripheral Mach number is $O(1)$. Comprehensive numerical solutions have been obtained for the full, time-dependent compressible Navier–Stokes equations. The details of the flow, temperature, and density evolution are described. In the early phase of spin-up, owing to the thermoacoustic disturbances caused by the compressible Rayleigh effect, the flows are oscillatory, and this oscillatory behaviour is pronounced at higher Mach numbers. The principal dynamical role of the Ekman layer is dominant over moderate times of orders of the homogeneous spin-up timescales. Owing to the density stratification in the radial direction, the Ekman layer is thicker in the central region of the interior. The interior azimuthal flows are mainly uniform in the axial direction. As the Mach number increases, the rate of spin-up in the interior becomes slower, and the propagating shear front is more diffusive. Explicit comparisons with the results for an infinite cylinder are made to ascertain the contributions of the endwall disks. In contrast to the usual incompressible spin-up from rest, the viscous effects are relatively more important for the case of a compressible fluid.

1. Introduction

Spin-up refers to a general class of transient motion of a confined fluid in response to an externally imposed change in the rotation rate of the container. The classical treatise of Greenspan & Howard (1963) dealt with the linearized spin-up flows that occur during transition from the initial rotation rate $\Omega-\Delta\Omega$ to the final rate Ω, where the Rossby number $\epsilon \equiv \Delta\Omega/\Omega$ was assumed to be infinitesimally small. Here, the flows of interest are characterized by the smallness of the reference Ekman number, $E \equiv \mu/\rho_0 \Omega H^2$, where μ is the reference viscosity of the fluid, ρ_0 the reference density, and H the characteristic length of the container. For the basic problem of linearized spin-up from an initial non-zero rotation rate, Greenspan & Howard showed that the crucial element in transient fluid dynamics is the formation of Ekman layers on the endwall disks. Owing to the radially outward motion in the Ekman layers, the fluid is drawn from the interior region (Ekman suction mechanism), which in turn leads to a radially inward meridional circulation in the interior. This meridional circulation in the bulk of the interior, where the direct effects of viscosity are small, spins the fluid up by angular momentum advection and vortex-line stretching. This elegant analytical account has since occupied the centrestage for modern studies of spin-up in a container.

One canonical problem of strongly nonlinear processes is spin-up from an initial state of rest to a finite rotation rate Ω. In this case, the above-defined Rossby number is unity, and the transient flow entails rather complex features that are unique to such nonlinear dynamics. Wedemeyer (1964), expanding many of the basic ideas of Greenspan & Howard, derived an approximate formulation to tackle the transient behaviour of the dominant azimuthal velocity in the interior. Specifically, for a cylindrical container (radius L and height H) of aspect ratio $H/L \approx O(1)$, Wedemeyer's model demonstrated that the interior flow is divided into two distinct regions separated by a velocity shear front which is propagating radially inward. The essential role played by the Ekman-layer suction mechanism was clearly delineated: as remarked earlier, the meridional circulation, driven by the Ekman-layer pumping, brings about the overall adjustment of the interior fluid. The timescale for global accomplishment of spin-up is given by $E^{-\frac{1}{2}}\Omega^{-1}$, which conforms with the earlier linearized predictions of Greenspan & Howard. The qualitative validity as well as the quantitative accuracy of the results of the Wedemeyer model have since been thoroughly discussed in a number of different experimental and numerical contexts (e.g. Watkins & Hussey 1973, 1977; Weidman 1976; Kitchen 1980; Hyun *et al.* 1983; Choi, Kim & Hyun 1989).

Most spin-up studies to date have almost exclusively been concerned with incompressible fluids. The early investigations of Greenspan & Howard (1963) and Wedemeyer (1964), as well as the later works cited above, addressed the problem of a homogeneous, incompressible fluid. Only preliminary studies were reported in the literature regarding the spin-up from rest of a stratified incompressible fluid (e.g. Greenspan 1980; Hyun 1983). These accounts of incompressible rotating fluids are highly relevant to geophysical fluid processes and other industrial applications. However, interest in the behaviour of a compressible fluid in a rapidly rotating environment has lately increased because of the connection with technological advances in high-powered gas centrifuges and turbomachinery. The extremely high rotational speed of these devices, of the order of 10000 r.p.m. and above (Sakurai & Matsuda 1974), implies that the compressibility effect, together with the strong density stratification that builds up in the direction perpendicular to the rotation axis, become vitally important for overall analyses of the transient motion of a compressible fluid.

As succinctly pointed out by Sakurai & Matsuda (1974), one immediate consequence of such rapidly rotating gas flows is that the conventional Boussinesq-fluid assumption is no longer applicable. Some of the general steady-state features of the fundamental aspects of the gasdynamics under strong rotation were disclosed by several analytical approaches, notably by for example Sakurai & Matsuda (1974), Bark, Meijer & Cohen (1978), Ungarish & Israeli (1984) and Park & Hyun (1990, 1991). The topic of transient flows of a gas under extremely high rotation is a comparatively new discipline (e.g. Bark *et al.* 1978), despite the fact that the subject is of intrinsic interest in basic fluid dynamics as well as in engineering applications. It appears that, based on a literature survey, the fundamental subject of spin-up flows from rest, with substantial compressibility effects incorporated, has not been properly described.

We propose in this paper to focus on the spin-up flow from rest of a gas in a rapidly rotating cylinder. As is intuitively obvious, there are certain similarities between the present problem and the much-studied counterpart of an incompressible, homogeneous fluid. However, it is equally important to recognize the differences between the two flows. In the case of a gas under rapid rotation, owing to the fluid

compressibility and the establishment of density stratification in the radial direction, dynamic features germane to the gas flows are eminent. These features give rise to additional complexities, which have hitherto not been shown explicitly in the published literature.

In the present study, we shall report on comprehensive results derived from numerical solutions to the governing full, time-dependent, compressible Navier–Stokes equations. In view of the extremely high rotation rates, direct experimental measurements are virtually non-existent. To the best of our knowledge, no conclusive analytical methodology has been successfully utilized to tackle these highly nonlinear, time-dependent fluid flows. It should be mentioned that Bark *et al.* (1978) explored several physically insightful linearized flow models, from the initial state of a pre-existing rotation, of a gas under strong rotation using asymptotic perturbation techniques. However, in the light of the overriding difficulties associated with analytical endeavours, full-scale numerical solutions promise to be a powerful alternative to capture the essentials of the transient flow characteristics. Past numerical simulations have been severely constrained by the requirement of prohibitively large computing resources as well as the formidable difficulties in constructing a reliable numerical code. We shall now take advantage of recent advances in computing capabilities, which have permitted full numerical simulations of the flow at hand.

In this paper, extensive numerical results will be presented to portray the details of the transient flow structure. Systematic computational analyses have been made of the time-dependent dominant azimuthal flows using three different values of the peripheral Mach number, $M = 1.0$, 3.0, 5.0. The concomitant meridional flows are depicted. These disclose the dynamic roles played by the thermoacoustic modes as well as the profound effects of the radial density stratification build-up on the Ekman pumping mechanism and their interactions. Major new physics pertinent to transient gas flows in a rapidly rotating container will thus be identified and plausible physical explanations are given. Although there may be some dependence of the compressible spin-up timescale on the Mach number, the level of understanding derivable from the present numerical results is restricted to homogeneous incompressible spin-up timescale ($E^{-\frac{1}{2}}\Omega^{-1}$).

Reference should be made to the recent works of Hyun & Park (1989) and Park & Hyun (1989). They give the complete numerical solutions of the spin-up flows of a gas in a rapidly rotating infinite cylinder. Evidently, the infinite cylinder is an artifact to restrict the analysis to the dynamic mechanisms, excluding the contributions by the Ekman layers on the endwall disks. This preceding work clearly demonstrated that the flow behaviour is mainly controlled by the compressible Rayleigh effect and the curvature effect. Also, the significance of the parameter group EM ($\equiv Kn$, the Knudsen number) has been pointed out. The present study is an extention to these papers in that a finite, closed cylinder is now considered. This will introduce the flow elements that are caused by the contributions from the Ekman layers on the endwall disks.

2. The model

Consider a perfect gas in a finite closed cylinder of radius L and height H. At the initial state, the gas is motionless at uniform temperature T_0 and density ρ_0. The relevant thermophysical properties of the gas are: μ, dynamic viscosity; κ, thermal conductivity; C_p, specific heat at constant pressure; C_v, specific heat at constant

volume; R, gas constant; $\gamma \equiv C_p/C_v$. These properties are taken to be constant. At the initial instant $t = 0$, the cylinder impulsively starts spinning about its central axis, which coincides with the z-axis, at angular frequency Ω. The subsequent axisymmetric motion of the gas is governed by the full, time-dependent, compressible Navier–Stokes equations. For convenience, we shall employ cylindrical coordinates (r, θ, z), with the corresponding velocity components (u, v', w), viewed in the rotating frame. These equations, expressed in non-dimensional conservative form, are

$$\frac{\mathrm{D}\rho}{\mathrm{D}t} = 0, \tag{1}$$

$$\frac{\mathrm{D}(\rho u)}{\mathrm{D}t} - \rho r - \rho v'\left(2 + \frac{v'}{r}\right) = -\frac{1}{\gamma M^2}\frac{\partial p}{\partial r} + E\left(\mathrm{L}u + \frac{1}{3}\frac{\partial Q}{\partial r}\right), \tag{2}$$

$$\frac{\mathrm{D}(\rho v')}{\mathrm{D}t} + \rho u\left(2 + \frac{v'}{r}\right) = E\mathrm{L}v', \tag{3}$$

$$\frac{\mathrm{D}(\rho w)}{\mathrm{D}t} = -\frac{1}{\gamma M^2}\frac{\partial p}{\partial z} + E\left(\nabla^2 w + \frac{1}{3}\frac{\partial Q}{\partial z}\right), \tag{4}$$

$$\frac{\mathrm{D}(\rho T)}{\mathrm{D}t} + (\gamma - 1)\rho T Q = \frac{\gamma E}{\sigma}\nabla^2 T + (\gamma - 1)\gamma M^2 E\Phi, \tag{5}$$

$$p = \rho T, \tag{6}$$

in which

$$\frac{\mathrm{D}}{\mathrm{D}t} = \frac{\partial}{\partial t} + \nabla\cdot[(\,)\boldsymbol{q}], \quad \boldsymbol{q} = (u, v', w),$$

$$\nabla^2 = \frac{\partial}{\partial r^2} + \frac{1}{r}\frac{\partial}{\partial r} + \frac{\partial^2}{\partial z^2}, \quad \mathrm{L} = \nabla^2 - \frac{1}{r^2}, \quad Q = \frac{1}{r}\frac{\partial (ru)}{\partial r} + \frac{\partial w}{\partial z},$$

$$\Phi = 2\left[\left(\frac{\partial u}{\partial r}\right)^2 + \left(\frac{u}{r}\right)^2 + \left(\frac{\partial w}{\partial z}\right)^2\right] + \left(\frac{\partial v'}{\partial r} - \frac{v'}{r}\right)^2 + \left(\frac{\partial v'}{\partial z}\right)^2 + \left(\frac{\partial w}{\partial r} + \frac{\partial u}{\partial z}\right)^2 - \tfrac{2}{3}Q^2.$$

The above equations were made dimensionless by using Ω^{-1}, L, T_0, ρ_0, $p_0 \equiv \rho_0 R T_0$ as the reference values for time, length, temperature, density and pressure, respectively. The significant non-dimensional parameters are

$E \equiv (\mu/\rho_0)/\Omega L^2$, the Ekman number;

$M \equiv \Omega L/(\gamma R T_0)^{\frac{1}{2}}$, the peripheral Mach number;

$\sigma \equiv \mu C_p/\kappa$, the Prandtl number.

For a definitive problem formulation, we shall consider a cylinder of aspect ratio $A = H/L = 1.0$. The origin of the coordinate system is located at the geometrical centre of the cylinder (see figure 1). Accordingly, the proper initial and boundary conditions can be stated as

$$u = w = 0, \quad v' = -r, \quad T = 1 \quad \text{at} \quad t = 0, \tag{7}$$

$$u = v' = w = 0 \quad \text{and} \quad T = 1 \quad \text{at} \quad z = 0.5 \quad \text{and} \quad r = 1.0 \quad (t > 0), \tag{8}$$

$$u = \frac{\partial}{\partial r}\left(\frac{v'}{r}\right) = \frac{\partial w}{\partial r} = \frac{\partial T}{\partial r} = 0 \quad \text{at} \quad r = 0, \tag{9}$$

$$\frac{\partial u}{\partial z} = \frac{\partial v'}{\partial z} = \frac{\partial T}{\partial z} = 0 \quad \text{and} \quad w = 0 \quad \text{at} \quad z = 0. \tag{10}$$

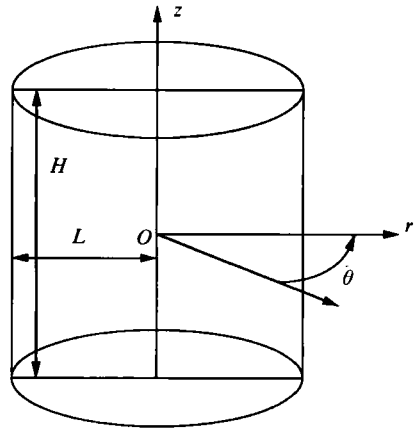

FIGURE 1. Schematic diagram of the coordinates.

3. Numerical method

We adopted an amended version of the finite-difference model originally developed by Harada (1980*a*, *b*). This model utilizes an explicit scheme of the Dufort–Frankel leapfrog type of second-order accuracy for both the time derivative and diffusion terms. The centred-differencing scheme of second-order accuracy is used for the space derivatives. The donor-cell technique is chosen for the convective terms to ensure numerical stability. The staggered grid arrangements are shown in figure 2.

In accordance with the finite-difference schemes of Harada (1980*a*, *b*), we have

$$(\bar{\rho}^{n+1}-\bar{\rho}^{n-1})/2\Delta t = -[\delta_r(\bar{\rho}u)^{n+1}+\delta_z(\bar{\rho}w)^{n+1}], \tag{11}$$

$$\frac{(\bar{\rho}u)^{n+1}-(\bar{\rho}u)^{n-1}}{2\Delta t} = -[\delta_r(\bar{\rho}uu)+\delta_z(\bar{\rho}wu)]^n+\left[\bar{\rho}\left(r+v'\left(2+\frac{v'}{r}\right)\right)\right]^n-\frac{1}{\gamma M^2}r\delta_r p^n$$
$$+Er\left[\frac{4}{3}\left(\delta_r\delta_r u^{\bar{n}}+\delta_r\left(\frac{u}{r}\right)^n\right)+\delta_z\delta_z u^{\bar{n}}+\tfrac{1}{3}\delta_r\delta_z w^n\right], \tag{12}$$

$$\frac{(\bar{\rho}v')^{n+1}-(\bar{\rho}v')^{n-1}}{2\Delta t} = -[\delta_r(\bar{\rho}uv')+\delta_z(\bar{\rho}wv')]^n-\left[\bar{\rho}u\left(2+\frac{v'}{r}\right)\right]^n$$
$$+Er\left[\delta_r\delta_r v'^{\bar{n}}+\delta_r\left(\frac{v'}{r}\right)^n+\delta_z\delta_z v'^{\bar{n}}\right], \tag{13}$$

$$\frac{(\bar{\rho}w)^{n+1}-(\bar{\rho}w)^{n-1}}{2\Delta t} = -[\delta_r(\bar{\rho}uw)+\delta_z(\bar{\rho}ww)]^n-\frac{1}{\gamma M^2}r\delta_z p^n$$
$$+Er\left[\delta_r\delta_r w^{\bar{n}}+\frac{1}{r}\delta_r w^n+\tfrac{4}{3}\delta_z\delta_z w^{\bar{n}}+\tfrac{1}{3}\delta_z\left(\frac{1}{r}\delta_r(ru)^n\right)\right], \tag{14}$$

$$\frac{(\bar{\rho}T)^{n+1}-(\bar{\rho}T)^{n-1}}{2\Delta t} = -[\delta_r(\bar{\rho}u)^{n+1}T^n+\delta_z(\bar{\rho}w)^{n+1}T^n]-(\gamma-1)(\bar{\rho}T)^{n+1}\bar{Q}^n$$
$$+\frac{\gamma E}{\sigma}r\left[\delta_r\delta_r T^{\bar{n}}+\frac{1}{r}\delta_r T^n+\delta_z\delta_z T^{\bar{n}}\right]+(\gamma-1)\gamma M^2 Er\,\bar{\Phi}^n, \tag{15}$$

$$p^{n+1} = (\bar{\rho}T)^{n+1}/r, \tag{16}$$

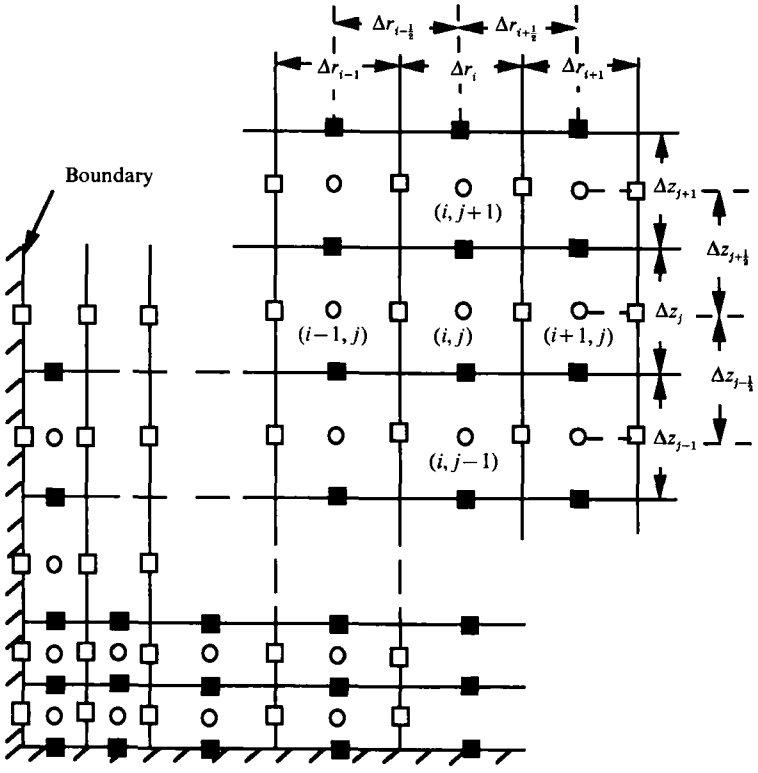

FIGURE 2. The arrangement of grid points $\bar{\rho}$ and T are defined at ○; u (or $\bar{\rho}u$) and v' (or $\bar{\rho}v'$) at □; w (or $\bar{\rho}w$) at ■. Note $\bar{\rho} \equiv \rho r$.

where

$$\left.\begin{aligned}
&\bar{\rho} \equiv \rho r, \quad \bar{Q} \equiv \frac{1}{r}\delta_r(ru) + \delta_z w \\
&\bar{\Phi} \equiv 2\left[(\delta_r u)^2 + \left(\frac{u}{r}\right)^2 + (\delta_z w)^2\right] + \left(\delta_r v' - \frac{v'}{r}\right)^2 + (\delta_z v')^2 + (\delta_r w + \delta_z u)^2 - \tfrac{2}{3}\bar{Q}^2, \\
&\delta_x \phi_i \equiv (\phi_{i-\frac{1}{2}} - \phi_{i-\frac{1}{2}})/\Delta x_i \\
&\delta_x \delta_x \phi_i^{\bar{n}} \equiv [(\phi_{i+1} - \bar{\phi}_i)/\Delta x_{i+\frac{1}{2}} - (\bar{\phi}_i - \phi_{i-1})/\Delta x_{i-\frac{1}{2}}]^n/\Delta x_i
\end{aligned}\right\} \tag{17}$$

with $\bar{\phi}_i^n = \frac{1}{2}(\phi_i^{n+1} + \phi_i^{n-1})$, $\Delta x_{i+\frac{1}{2}} = \frac{1}{2}(\Delta x_i + \Delta x_{i+1})$, $\Delta x_i = \frac{1}{2}(\Delta x_{i+\frac{1}{2}} + \Delta x_{i-\frac{1}{2}})$,

where ϕ represents a physical variable (such as $\bar{\rho}$ or $\bar{\rho}u$) and x denotes a coordinate.

The solution procedure is as follows:

(i) The mass velocities $(\rho u)^{n+1}$, $(\rho v')^{n+1}$, $(\rho w)^{n+1}$, are computed from (12)–(14).

(ii) The density ρ^{n+1} is computed from the continuity equation (11), using $(\rho u)^{n+1}$ and $(\rho w)^{n+1}$.

(iii) The pressure $P^{n+1}(= (\rho T)^{n+1})$ is obtained from the energy equation (16).

(iv) The values of u^{n+1}, v^{n+1}, w^{n+1} and T^{n+1} are obtained by driving the mass velocities and pressure by ρ^{n+1}.

(v) Steps (i)–(iv) are repeated with marching in time.

(vi) The time filtering is done every 20 cycles to avoid computational splitting caused by the leapfrog scheme: $\phi^{n+\frac{1}{2}} = \frac{1}{2}(\phi^n + \phi^{n+1})$.

(vii) Steps (i)–(vi) are repeated until the desired time instant.

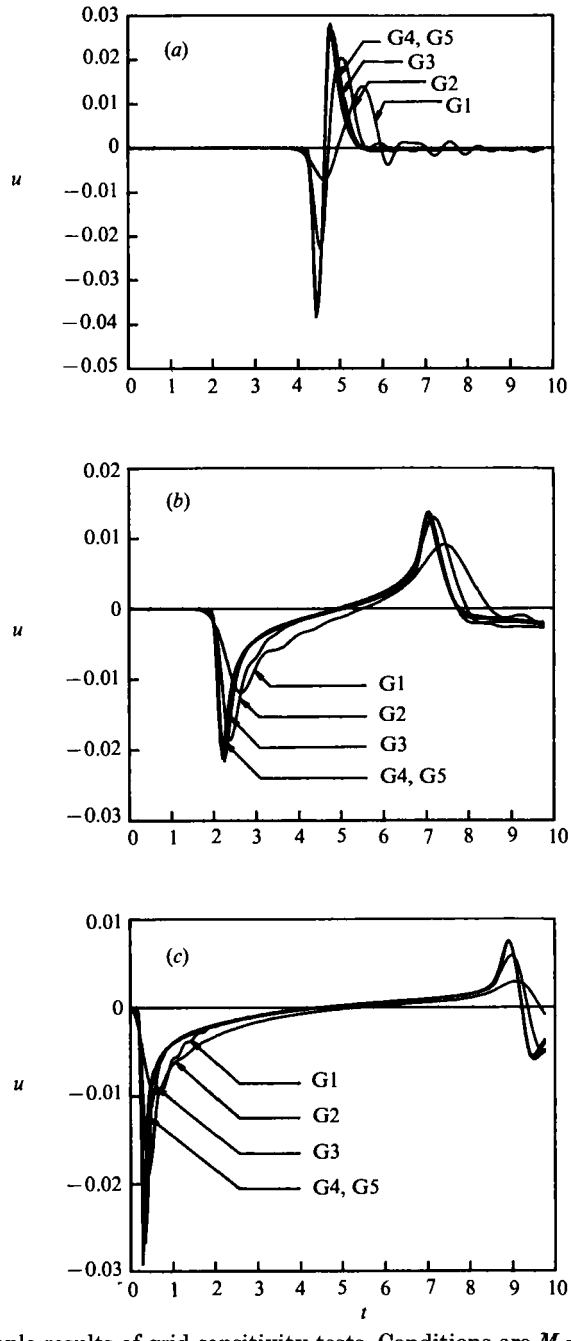

FIGURE 3. Example results of grid-sensitivity tests. Conditions are $M = 5.0$, $z = 0.1$ and the value of radial position is (*a*) $r = 0.05$; (*b*) $r = 0.55$; and (*c*) $r = 0.95$. The mesh networks are: G1(27 × 17), G2(52 × 19), G3(102 × 20), G4(152 × 22), G5(202 × 24).

The details of computational methodology for the numerical model are discussed by Harada (1980*a*, *b*). For the calculations, a mesh network of (102 × 20) in half of the (r, z) axial plane was typical. Suitable grid stretching was implemented to achieve higher resolution of the boundary layers. Extensive sensitivity tests on grid size were

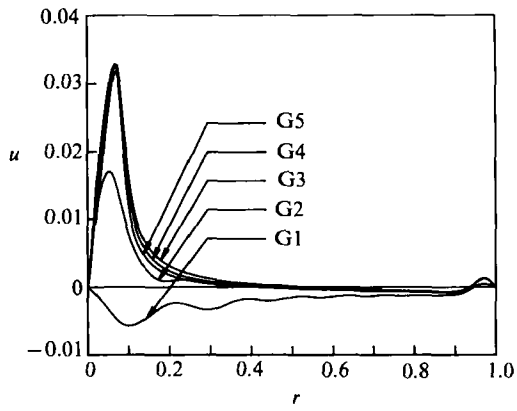

FIGURE 4. Example results of grid-sensitivity tests. Conditions are $M = 5.0$, $z = 0.1$, $t = 4.875$. The mesh networks are: G1(27 × 17), G2(52 × 19), G3(102 × 20), G4(152 × 22), G5(202 × 24).

performed for several example runs, and the overall results were satisfactory (see the examples in figures 3 and 4). The present numerical method is shown to be versatile and sufficiently robust to capture the major dynamical elements within the ranges of parameters in this study. The Rayleigh wave is not a strong shock wave for the peripheral Mach numbers adopted in the present work, $M < 5.0$. (A shock wave may be expected for very large peripheral Mach numbers, i.e. $M \geqslant 20.0$, see Harlow & Meixner 1961.) The Rayleigh wave in the present context can better be characterized as an acoustic wave (Hyun & Park 1989). Thus, in the present numerical model, no serious numerical difficulties, such as the shock capturing problem, were encountered. Considering both the computational stability and accuracy, the time interval Δt was chosen to range up to $\Delta t_{\max} = 0.0002$, which was found to be adequate to resolve the details of transient flows (see figure 4). All the computations were executed on a CRAY-2S supercomputer. For typical runs, approximately 10 h of CPU time were needed for a given set of parameters.

4. Results and discussion

As can be inferred from the non-dimensional governing equations, a given flow will be characterized primarily by four dimensionless parameters, E, M, σ_p and γ. For all the calculations covered in the present paper, $E = 10^{-4}$, $\sigma = 1.0$ and $\gamma = 1.2$. The choice of these parameter values renders the problem definition somewhat artificial. This study has been motivated by possible applications to a rapidly rotating gas centrifuge. The primary objective of this paper is, as asserted earlier, to reveal the lowest-order flow characteristics of compressible spin-up. The gross qualitative features of the results are not profoundly dependent on the choice of the exact values of σ and γ. The influence of the rapid rotation of the vessel, together with the compressibility effect, is reflected principally in the peripheral Mach number, M. Therefore, for specific quantitative comparisons of the computed results, complete flow details were acquired for three Mach numbers, $M = 1.0$, 3.0, 5.0. Note that the compressibility effect is proportional to M^2; henceforth, these three values of the Mach number roughly represent the characteristic ranges of $M^2 \approx O(1)$, $M^2 \approx O(10)$, $M^2 \geqslant O(20)$. In the ensuing discussing, we shall use the absolute azimuthal velocity, $v = v' + r$. Since the problem is symmetric with respect to the cavity mid-height $z = 0$, the results will be displayed only in the upper-half of the cylinder, $0 \leqslant z \leqslant 0.5$,

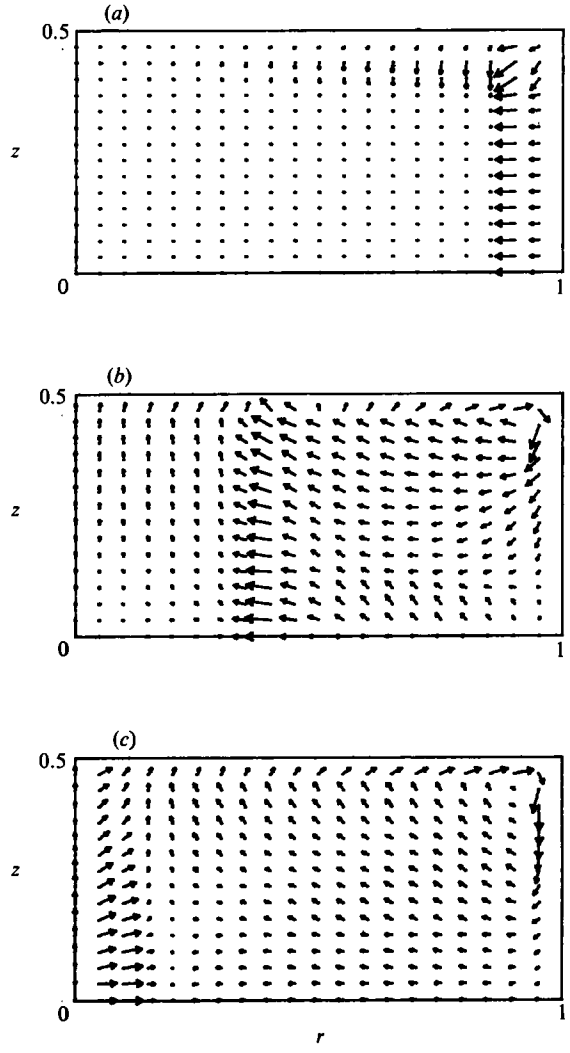

FIGURE 5. Vector plots on the meridional plane at early times: (*a*) $t = 0.49$; (*b*) $t = 2.95$; (*c*) $t = 4.99$. $M = 5.0$.

$0 \leqslant r \leqslant 1.0$. In the present set of computations, the results are restricted to isothermal wall boundary conditions, which makes the computational formulation easier. An even more important reason is that the investigations by Bark *et al.* of linear spin-up used the constant temperature wall boundary condition, and one aim of the present effort is to extend their work to a strongly nonlinear regime. Results using different thermal wall conditions will be dealt with in separate papers. For steady-state problems, parallel calculations including the effect of the wall thermal boundary condition were reported by Park & Hyun (1990, 1991).

The explicit effect of fluid compressibility is best portrayed in the vector plots of meridional flows. Figure 5, depicting the numerical results for $M = 5.0$, illustrates the main characteristics of gas flows in the early phase of spin-up. As is apparent in figure 5(*a*), at small times compressible waves are observed to propagate radially inward from the sidewall periphery and vertically downward from the outer portion of the endwall disk. The abrupt start of the fast moving solid walls gives rise to viscous

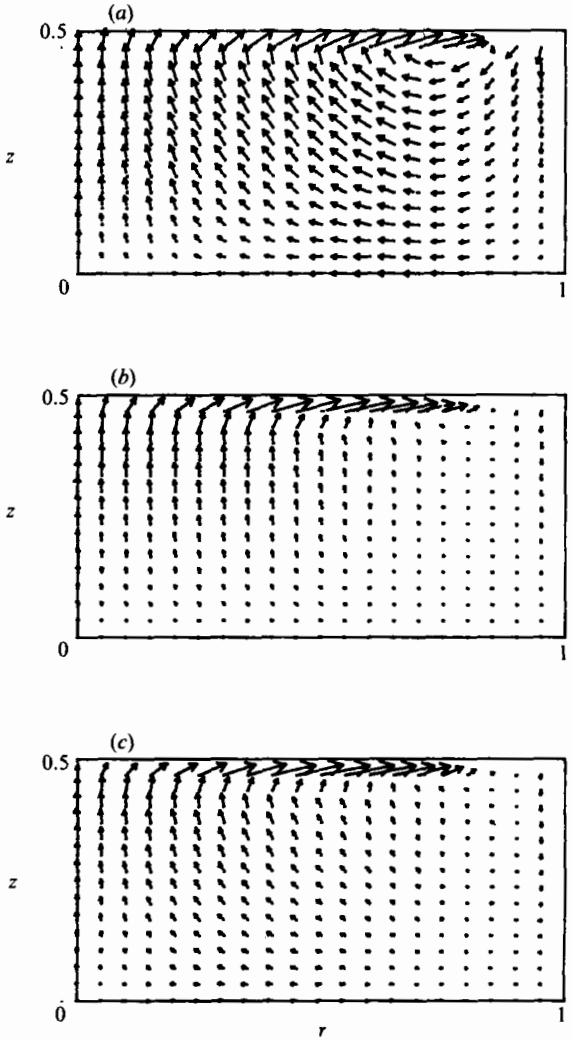

FIGURE 6. Vector plots on the meridional plane at intermediate times: (a) $t = 35.4$; (b) $t = 73.8$; (c) $t = 98.0$. $M = 5.0$.

heating of the adjacent fluid, which causes concomitant pressure variations and a velocity component normal to the walls. The flow of a gas induced by a suddenly started fast-moving solid wall, customarily termed the compressible Rayleigh problem, has been documented mostly through theoretical models for a flat plate (Howarth 1951; Stewartson 1955; Hanin 1960); Hyun & Park (1989) and Park & Hyun (1989) gave numerical solutions for this flow in a rotating cylindrical geometry. It is interesting to note in figure 5(a) that the vertically downward velocities near the top endwall disk increase in magnitude with radius. This reflects the fact that the strength of the compressible Rayleigh flow increases as the effective Mach number of the sliding solid wall increases.

At a later time instant, as shown in figure 5(b), the radially inward Rayleigh wave is seen to continue propagating toward the central axis; and the vertically downward Rayleigh wave has already reached the mid-height, been reflected at $z = 0$ and is then seen to move vertically upward in the regions slightly above the mid-height of

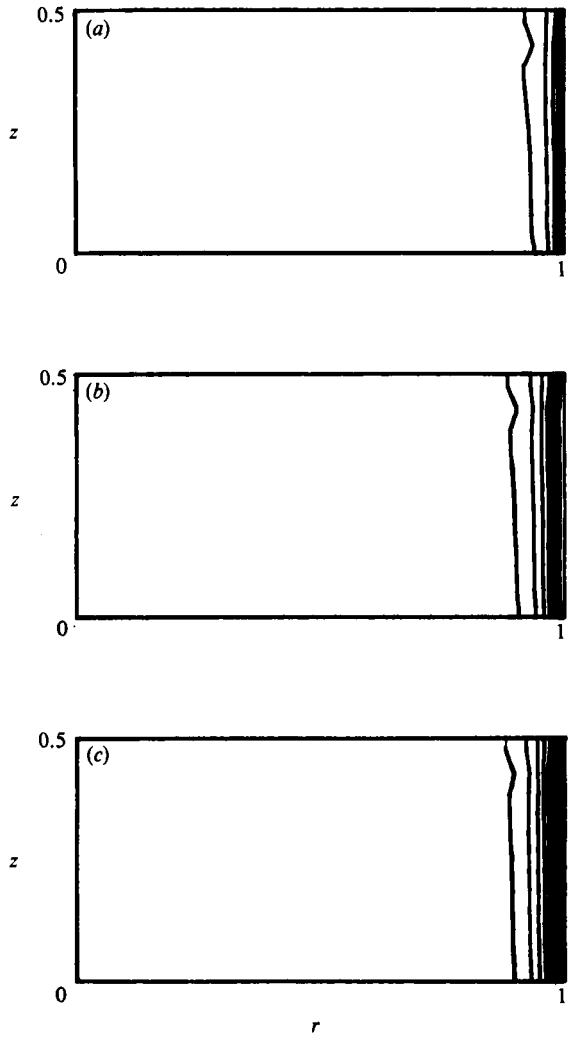

FIGURE 7. Evolution of the density field at times (*a*) $t = 35.4$; (*b*) $t = 73.8$; (*c*) $t = 98.0$. $M = 5.0$. The value of the leftmost contour is 1.0, and the contour interval is 0.5.

the cavity. In figure 5(*b*), the beginning of the formation of the Ekman layer at the endwall disk and of the sidewall layer at the sidewall periphery is observed. A still later time instant, figure 5(*c*) shows the reflection of the radially propagating Rayleigh waves at the central axis. As pointed out by Hyun & Park (1989), the existence of the Rayleigh waves is a salient feature of the very early stage of spin-up; the Rayleigh waves are produced in a compressible fluid by strong shearing motion of an impulsively started solid plate. Since the cylinder is finite and capped by the endwall disks, the overall flow field in the interior during the early phase displays a combination of the compressible Rayleigh effect and the early-time behaviour of the Ekman-layer-induced meridional flows. With further passage of time, the Ekman layers are strengthened, and the compressible Rayleigh effect is gradually outweighed by the meridional flows driven by the Ekman-layer pumping mechanism.

Extending the calculations, figure 6 shows vector plots of meridional flows at moderate times of order of the homogeneous spin-up timescale $O(E^{-\frac{1}{2}}\Omega^{-1})$. At this

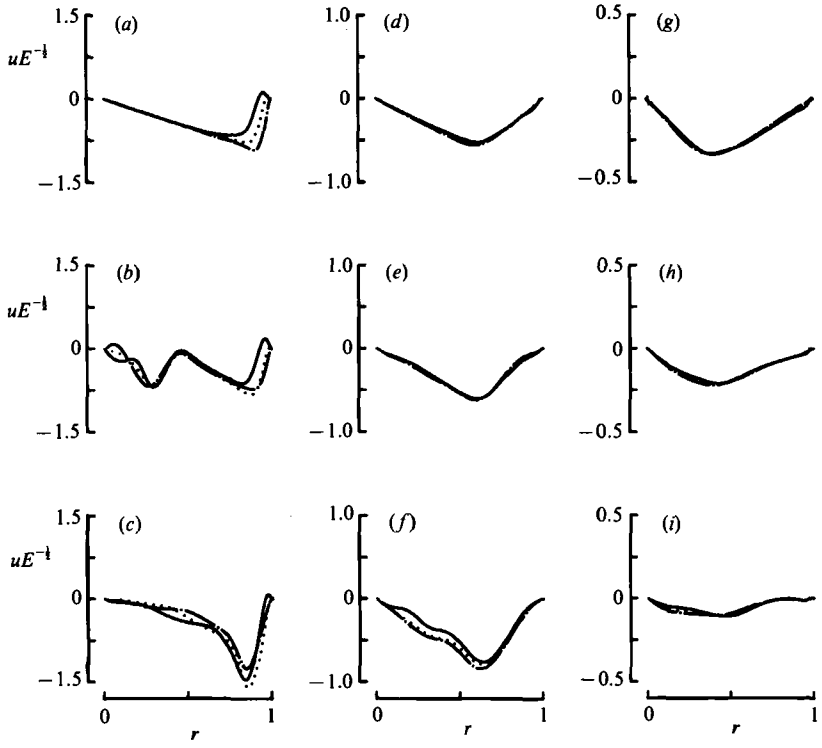

FIGURE 8. Structure of the radial velocity field, u. The axial positions are: ——, $z = 0.073$; · · ·, $z = 0.19$; —·—, $z = 0.31$. The Mach numbers are $M = 1.0$ for the top row, $M = 3.0$ for the middle row, and $M = 5.0$ for the bottom row. Times are $t = 4.99$ for the left column, $t = 35.4$ for the middle column, and $t = 73.8$ for the right column.

intermediate stage, the compressible flows exhibit two distinctively different aspects in comparison to the incompressible flows. One notable feature of compressible flows is the build-up of a radial density stratification, strongly established within this time span. Because of the preponderance of density effects at larger radii, the meridional velocities in these regions are, in general, reduced to achieve global mass continuity in the cavity. Consequently, as spin-up progresses, the magnitude of the meridional velocities tend to decrease in the outer high-density region; these changes in velocities are noticeable as the compressibility effect becomes appreciable. Another feature is the oscillatory nature of the meridional flows: the radially inward flow in much of the cavity interior is conspicuous in figure 6(*a*, *c*), whereas such radially inward motions are very weak in figure 6(*b*). This implies that there is an oscillatory element of meridional flow superimposed on the general adjustment process.

In conjunction with the adjustment of the velocity field, it is of interest to examine the behaviour of the density field in response to the abrupt rotation of the container. Figure 7 shows how the density stratification, predominantly in the radial direction, is established in the course of the spin-up process. It is clearly shown that the concentration of fluid mass in the peripheral region of the container is pronounced.

Exploiting the wealth of numerical data, the profiles of different velocity components at different times are illustrated in figures 8–10. The u-profiles at small times, as shown in figure 8(*a*–*c*), exhibit axial variations, although the variations are relatively small in magnitude. This is attributable to the meridional motions which are caused by the downward compressible Rayleigh waves emanating from the top

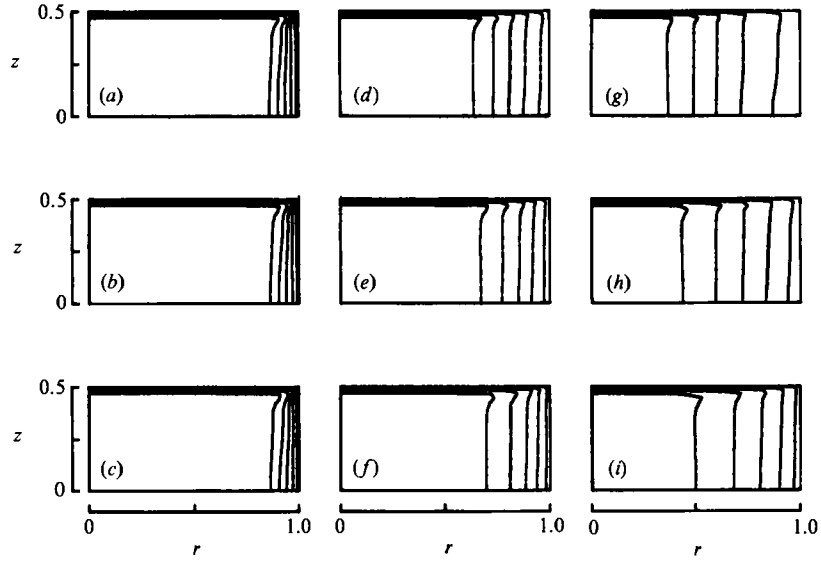

FIGURE 9. Evolution of the angular velocity fields, v/r. The contour values are 0.1, 0.3, 0.5, 0.7 and 0.9, beginning from the leftmost contour. The Mach numbers are $M = 1.0$ for the top row, $M = 3.0$ for the middle row, and $M = 5.0$ for the bottom row. Times are $t = 4.99$ for the left column, $t = 35.4$ for the middle column, and $t = 73.8$ for the right column.

endwall disk. Owing to the presence of this meridional flow, the u-velocities display axial variations in the very early phase of spin-up. As emphasized in figures 5 and 6, compressible Rayleigh waves play a central role in determining the principal character of the early-time behaviour of meridional flows. Figure 8 also demonstrates that the radial velocities weaken considerably with time; after times of order of the homogeneous spin-up timescale, the magnitude of u decreases to small values (note the difference in scales for the ordinates in figure 8). The dominant azimuthal velocities v are substantially uniform in the axial direction in the bulk of the interior flow field. The evolution of the global azimuthal flow fields are portrayed in figure 9 in the form of contour maps. The profiles of the axial velocities w indicate the nature of the meridional flows induced by the Ekman layers. As shown in figure 10, the overall axial velocities are directed toward the endwalls disks at radii smaller than (ahead of) the propagating shear front, and are directed toward the mid-height at radii larger than (behind) the front. This is qualitatively consistent with the well-documented behaviour of the meridional flows that occur in spin-up from rest of an incompressible fluid. One noteworthy feature of compressible flows is the radial variation of the thickess of the Ekman layer. As can be seen in figure 10, the Ekman layer is thickner in the central portion near the axis. This can be explained by noting that, owing to the presence of a strong radial stratification, in particular, at large times, the fluid in the central portion becomes rarefied. Under the assumption that μ remains constant, the local viscous effects, measured by the kinematic viscosity, $\nu = \mu/\rho$, become large at small radii. The thicker Ekman layer in the central portions is indicative of the enhanced viscous effects in these low-density regions. As stated by Bark *et al.* (1978), the thickness of the Ekman layer is scaled by $E_1^{\frac{1}{4}}$, where $E_1 \equiv \mu/(\rho\Omega L^2)$ denotes the local Ekman number.

In order to gain further physical insight into the transient flow details, the time histories of the meridional velocities are recorded at a representative location in figure 11 for u and in figure 12 for w. The oscillatory behaviour, superposed on the

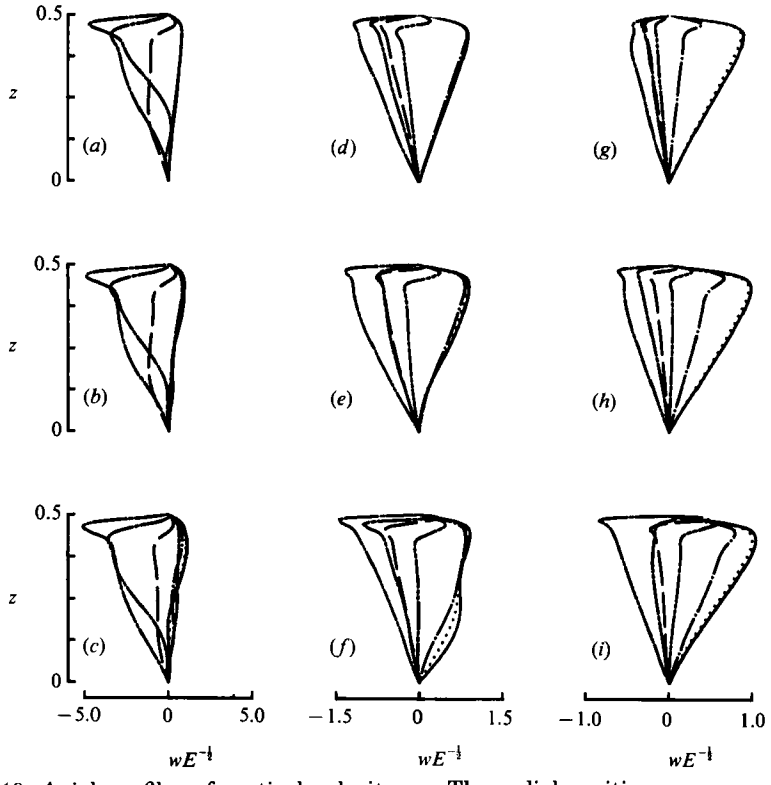

FIGURE 10. Axial profiles of vertical velocity, w. The radial positions are: ——, $r = 0.09$; · · ·, $r = 0.24$; —·—, $r = 0.49$; — — —, $r = 0.74$; – – –, $r = 0.89$; ——, $r = 0.94$; —· ·—, $r = 0.97$. The Mach numbers are $M = 1.0$ for the top row, $M = 3.0$ for the middle row, and $M = 5.0$ for the bottom row. Times are $t = 4.99$ for the left column, $t = 35.4$ for the middle column, and $t = 73.8$ for the right column.

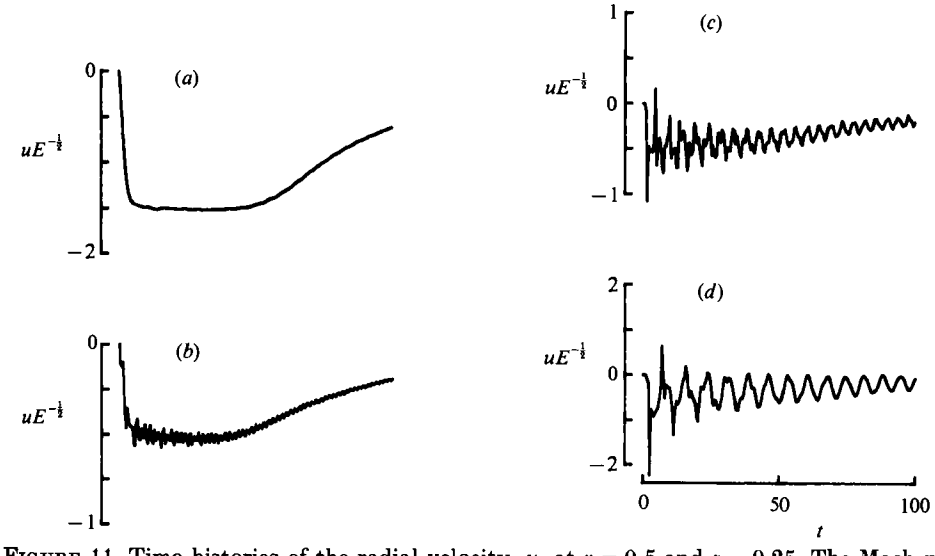

FIGURE 11. Time histories of the radial velocity, u, at $r = 0.5$ and $z = 0.25$. The Mach numbers are: (a) incompressible fluid; (b) $M = 1.0$; (c) $M = 3.0$; (d) $M = 5.0$.

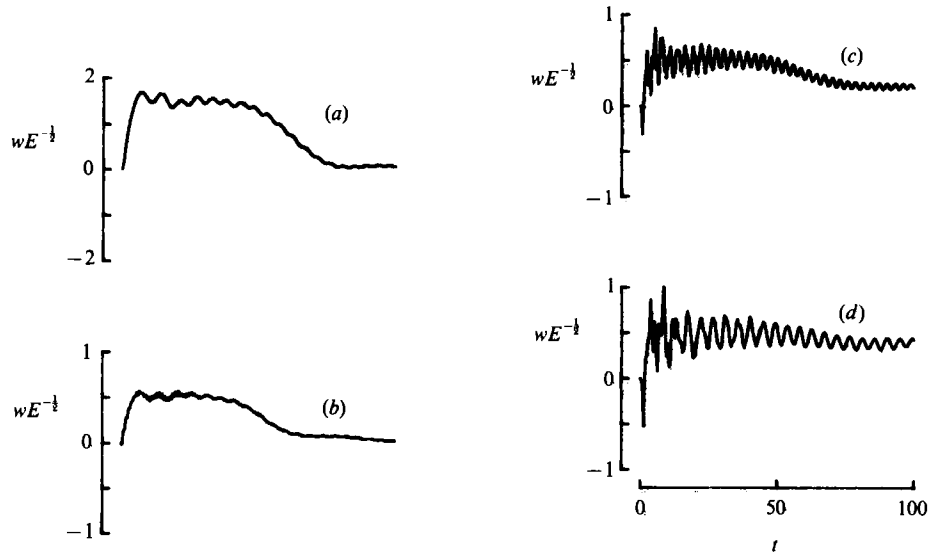

FIGURE 12. Time histories of the vertical velocity, w, at $r = 0.5$ and $z = 0.25$. The Mach numbers are: (*a*) incompressible fluid; (*b*) $M = 1.0$; (*c*) $M = 3.0$; (*d*) $M = 5.0$.

overall approach to the final state, is apparent. As shown in the preceding analyses (Hanin 1960; Harlow & Meixner 1961; Hyun & Park 1989; Park & Hyun 1989), this oscillatory nature is attributable to the presence of the propagating disturbances which are induced by viscous heating generated at the solid boundaries by the abrupt start of the rotating container. These disturbances are thermoacoustic in nature, and, the non-dimensional period of oscillation of these propagating disturbances through the compressible medium has been shown by the above-cited authors to be $O(M)$. Based on similar reasoning, in the case of the w-plots in figure 12 the non-dimensional period of oscillation is given by $O(M\frac{1}{2}A)$, since the (dimensional) axial distance that the disturbances travel before being reflected at the mid height is $(L\frac{1}{2}A)$. It should be noted from figure 12(*a*) that oscillations are discernible for an incompressible fluid. However, this oscillation is due to the inertial oscillation, which has been well explained in previous studies (Kitchen 1980, Warn-Varnas *et al.* 1978). For compressible fluids, these inertial oscillations are also present. However, the relative strength of the inertial oscillations in comparison to the Rayleigh wave decreases rapidly as the compressibility effect increases. In figure 12(*d*) for $M = 5.0$, for example, the inertial oscillation is overshadowed by the dominant Rayleigh wave. Inspection of the u- and w-plots in figures 11 and 12 corroborates the above argument regarding the period of the oscillation approach to the final state. The amplitude of the oscillation depends mainly on the strength of the imposed thermal load on the boundary, which is the direct source of viscous heating of the compressible fluid at the solid walls. As is evident in figures 11 and 12, the amplitude of oscillation grows as M increases, which is in accord with the previous general analyses (Hyun & Park 1989). Summarizing the computational results for the meridional velocities, one significant conclusion is that the general spin-up process may be characterized by an oscillatory approach, superposed on the overall system-wide adjustment, to the final state. This oscillatory behaviour is more pronounced at high Mach numbers. Consequently, an additional dimensional timescale, $M\Omega^{-1}$, is meaningful for compressible flows in order to correctly depict the transient states of spin-up from rest.

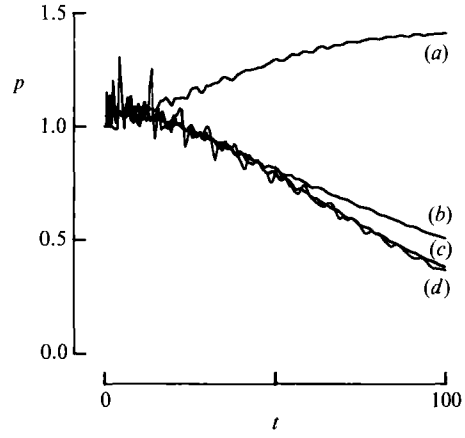

FIGURE 13. Time histories of the pressure, p, at axial position $z = 0.25$. The radial positions are (a) $r = 0.9$; (b) $r = 0.7$; (c) $r = 0.5$; (d) $r = 0.04$.

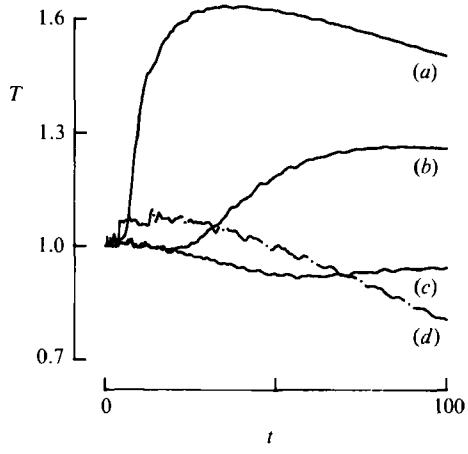

FIGURE 14. Time histories of the temperature, T, at axial position $z = 0.25$. The radial positions are (a) $r = 0.9$; (b) $r = 0.7$; (c) $r = 0.5$; (d) $r = 0.04$.

In parallel with the examination of the meridional flow structure, it is advantageous to examine the radial pressure distribution as spin-up progresses. Figure 13 depicts the response of the pressure field. At locations very close to the sidewall periphery (see curve *a*), a rather monotonic build-up of pressure, due to centrifugal compression, is evident. However, in the interior regions slightly away from the sidewall, the pressure decreases fairly monotonically with time owing to the rarefaction in these areas (see curves *b*, *c*, *d*). The overall temporal evolution of the pressure field contains the small-scale thermoacoustic oscillations. In particular, near the central axis, the incoming and reflected disturbances combine to yield appreciable peaks (see curve *d*). As was asserted previously (Hyun & Park 1989; Park & Hyun 1989), the amplitudes of these oscillations are appreciable at early phases but they decay gradually afterward.

The evolution of the temperature field is presented in figure 14. In the regions very close to the sidewall periphery (see curve *a*), the sudden rotation of the container wall creates large gradients of the azimuthal flows. Owing to the associated viscous heating, the temperature quickly rises to a high value. As time elapses, the velocity

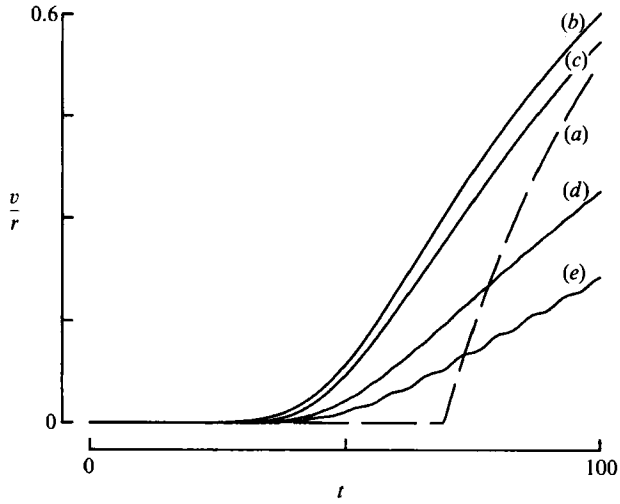

FIGURE 15. Time histories of the angular velocities, v/r, at $r = 0.5$ and $z = 0.25$. (*a*) Solution of the incompressible Wedemeyer model; (*b*) incompressible Navier–Stokes solution; (*c*) $M = 1.0$; (*d*) $M = 3.0$; (*e*) $M = 5.0$.

gradients, and consequently the viscous heating, are reduced; the temperature decreases slowly accordingly. In the vicinity of the axis (see curve *d*), at small times the arrival and reflection of the thermoacoustic disturbances is responsible for the small increase of temperature. At intermediate and large times, the fluid becomes rarefied and thus slightly cooled.

The time histories of the dominant azimuthal velocity component, v, are displayed in figure 15 for three different Mach numbers. The location chosen for the plots is at mid-radius and a quarter-height away from the endwall, i.e. $r = 0.5$ and $z = 0.25$. Also shown in figure 15 is the result of the incompressible spin-up from rest, which was acquired by solving the full, incompressible time-dependent Navier–Stokes equations under the same geometrical conditions. For these incompressible homogeneous spin-up calculations, a numerical code was constructed following the well-established model of Warn-Varnas *et al.* (1978). For comparisons, the solution based on the classical Wedemayer (1964) model for the incompressible spin-up from rest is also included in figure 15. First, it is shown that the general rate of spin-up is slower as the compressibility effect increases. The propagation speed of the shear front, separating the non-rotating fluid and the spun-up fluid, is also slower as M increases. The existence of the thermoacoustically induced oscillatory modes is discernible for high-Mach-number flows. Scrutinity of the curve for $M = 5.0$ in figure 15 reconfirms the observation that the dimensional period of this oscillation is scaled with $O(M\Omega^{-1})$; this is consistent with the prior description of the meridional flow fields.

Figure 16 portrays time-sequence plots of radial profiles of the azimuthal velocity field along the quarter-height ($z = 0.25$). In view of the substantial axial uniformity of v in the bulk of the interior, these plots illustrate the general flow behaviour in much of the cavity. As the spin-up process progresses, a cylindrical shear front propagates radially inward. As remarked earlier, ahead of (at smaller radii than) the front, the fluid remains non-rotating. As shown in figure 16, the main differences in the gross characteristics of the evolving azimuthal flow field between incompressible and highly compressible flows are quantitative. The overall rate of spin-up is reduced

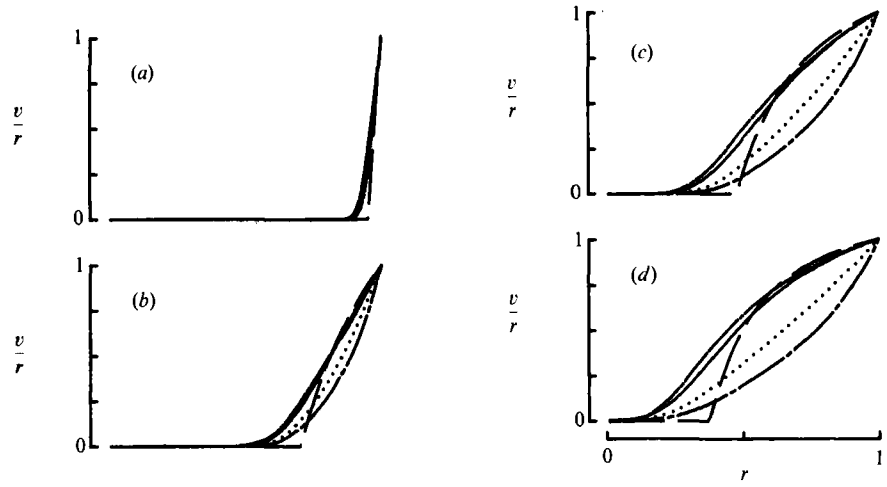

FIGURE 16. Radial profiles of the angular velocity, v/r, at axial location $z = 0.25$: ---, solution of the incompressible Wedemeyer model; —·—, incompressible Navier–Stokes solution; ——, $M = 1.0$; ....., $M = 3.0$; ———, $M = 5.0$. Times are: (*a*) $t = 4.99$; (*b*) $t = 35.4$; (*c*) $t = 73.8$; (*d*) $t = 98.0$.

at higher Mach numbers. Also noteworthy is that, as M increases, the shear front itself becomes less distinct; this suggests that the neighbourhood of the shear front is more diffusively controlled at high Mach numbers. For the case of incompressible spin-up, Hyun *et al.* (1983) ascertained that the shear-front area represents a localized region of intensified viscous effects. The implications of the present numerical results are that, as M increases, diffusive effects are more pronounced. The phenomenon is reflected in the overall retardation of the global spin-up process in the bulk of the interior. Also, the spatial gradients of the velocity field are milder, especially in the vicinity of the shear front.

In the case of an incompressible spin-up from rest in a closed container, the angular momentum is mainly convected by the action of the meridional circulation, which is induced by the Ekman-layer pumping at the endwall disks. The diffusive contribution of the peripheral sidewall to the global spin-up process is comparatively minor. However, in the case of highly compressible fluids, the attainment of angular momentum purely by the action of the cylindrical sidewall, owing to the compressible Rayleigh effect (Hanin 1960; Hyun & Park 1989; Park & Hyun 1989*a*), has also been shown to be substantial. It therefore appears that, for compressible spin-up in a closed container, the major mechanisms to be considered are the above two, i.e. the Ekman-layer-driven meridional circulation and the Rayleigh-flow effects emanating from the solid boundaries. It is immediately clear that separate evaluations of these two effects could lead to an identification of the relative importance of the prominent dynamic effects. For this purpose, explicit comparisons between the present results for a finite closed container and the results for an infinite cylinder are useful. An infinite cylindrical vessel is an artifact to isolate only the Rayleigh flow effects from the peripheral wall since there is no contribution from endwall disks.

Figure 17 shows time histories of the angular velocity for both a finite closed cylinder and an infinite cylinder: the spin-up proceeds at faster rates in a closed finite cylinder than in an infinite one. The difference between the two curves represents all the dynamic effects associated with the presence of the endwall disks. In the interior core region (see figure 17*a*), the principal drive for spin-up is based on the Ekman

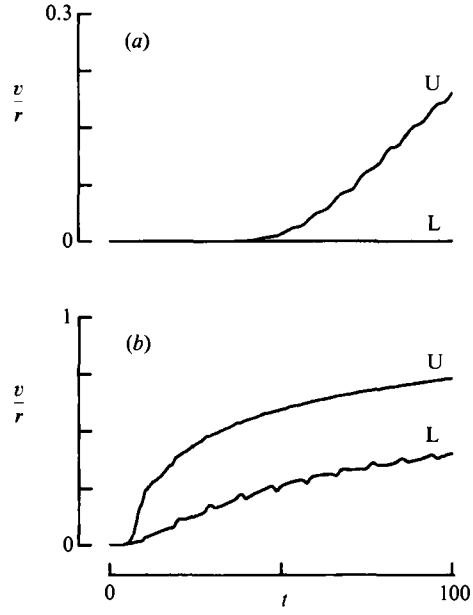

FIGURE 17. Comparisons of the angular velocities, v/r, between the solutions of a finite closed cylinder of $A = 1.0$ (shown by U) and of an infinite cylinder (shown by L). $M = 5.0$ and $E = 10^{-4}$. The axial position of the finite cylinder is $z = 0.25$. The radial positions are: (*a*) $r = 0.5$; (*b*) $r = 0.9$.

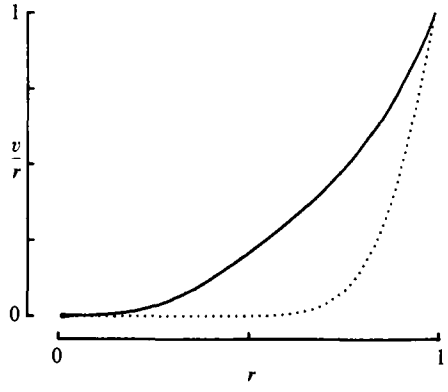

FIGURE 18. Angular velocity, v/r, for a finite, closed cylinder of $A = 1.0$ (shown by solid line) and an infinite cylinder (shown by dotted line). $M = 5.0$, $E = 10^{-4}$, $t = 98.0$. The axial position of the finite cylinder is $z = 0.25$.

layer on the endwall disks. The diffusion from the periphery is small at this far interior location. However, for compressible spin-up, the contribution based on the Rayleigh effect, primarily derivable from the sidewall, is significant in the regions close to the periphery (see figure 17*b* for $r = 0.9$). For an infinite cylinder, the spin-up process is driven mostly by diffusion from the abruptly started cylindrical sidewall. The presence of the thermoacoustically excited oscillations is more pronounced in the case of an infinite cylinder. As is evident in figure 17, at large radii the Rayleigh-flow effects are certainly of the same order of magnitude as the endwall disk-related dynamic effects (note the difference in scales of the ordinates in figures 17 (*a*) and 17 (*b*). This is in contrast to the case of incompressible spin-up; it is stressed

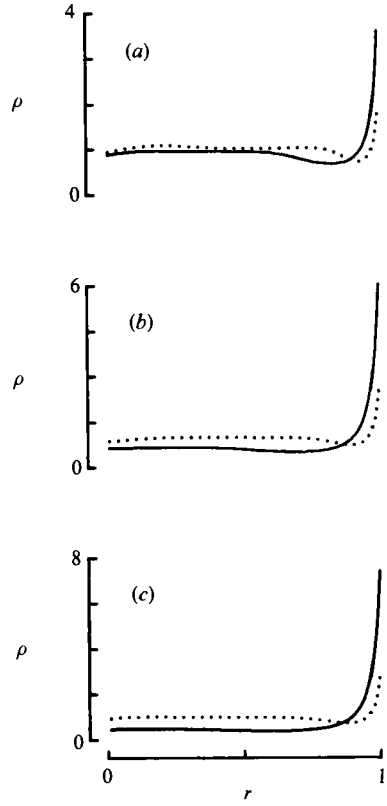

FIGURE 19. Density, ρ, for a finite, closed cylinder of $A = 1.0$ (shown by solid line) and an infinite cylinder (shown by dotted line). $M = 5.0$ and $E = 10^4$. The axial position of the finite cylinder is $z = 0$. Times are: (*a*) $t = 35.4$; (*b*) $t = 73.8$; (*c*) $t = 98.0$.

that, for an incompressible flow, the contributions resulting from the diffusive effects from the solid boundaries are minor over the timescales $E^{-\frac{1}{2}}\Omega^{-1}$, as was ascertained by numerical simulations of Hyun *et al.* (1983), among others.

A comparison of the radial profiles of angular velocity for a finite closed cylinder and an infinite cylinder are displayed in figure 18. Once again, the difference between the two results reflects the dynamic effects of the endwall disks. The radial profiles of density for the two cases are plotted in figure 19 (note the difference in scales of the ordinates). It is clearly seen that the attainment of radial stratification in the vicinity of the sidewall during the course of spin-up is substantially more effective in a closed cylinder. For both cases, the asymptotic approach to the final state is described by Bark *et al.* (1978)

$$\rho(r)/\rho(1) = \exp\{\tfrac{1}{2}\gamma M^2(r^2 - 1.0)\}.$$

5. Conclusions

Extensive numerical solutions to the full, time-dependent compressible Navier–Stokes equations have been analysed for impulsive spin-up from rest of gas contained in a cylinder. Throughout the transient evolution, the dominant azimuthal velocities in the interior are mainly uniform in the axial direction. The homogeneous spin-up timescale characterizes the global adjustment process of the azimuthal flow.

As the peripheral Mach number, M, increases, the propagating velocity-shear frontal zone is more diffusive, and the rate of spin-up decreass. In the early phase of spin-up, the presence of thermoacoustic disturbances, stemming from the compressible Rayleigh effect, is in evidence. This oscillatory behaviour is more pronounced as M increases. The strong density stratification in the radial direction is noted at large M. Consequently, the fluid in the central portions tends to be rarefied, resulting in enhanced viscous effects in those areas. A short time after the cylinder is set into motion, the thickness of the Ekman layer increases as radius decreases, but the Ekman layer ultimately disappears as the final state of solid-body rotation is approached.

This work was supported in part by research grants from Korean Science & Engineering Foundation. The support by the Advanced Fluid Engineering Research Center (AFERC) of Pohang Institute of Science & Technology is appreciated.

REFERENCES

BARK, F. H., MEIJER, P. S. & COHEN, H. I. 1978 Spin-up of a rapidly rotating gas. *Phys. Fluids* **21**, 531–539.

CHOI, S., KIM, J. W. & HYUN, J. M. 1989 Transient free surface shape in an abruptly rotating, partially-filled cylinder. *Trans. ASME* I: *J. Fluids Engng* **111**, 439–442.

GREENSPAN, H. P. 1980 A note on the spin-up from rest of a stratified fluid. *Geophys. Astrophys. Fluid Dyn.* **15**, 1–5.

GREENSPAN, H. P. & HOWARD, L. N. 1963 On a time-dependent motion of a rotating fluid. *J. Fluid Mech.* **17**, 385–404.

HANIN, M. 1960 On Rayleigh's problem for a compressible fluid. *Q. J. Mech. Appl. Maths* **13**, 184–198.

HARADA, I. 1980*a* A numerical study of weakly compressible rotating flows in a gas centrifuge. *Nucl. Sci. Engng* **73**, 225–241.

HARADA, I. 1980*b* Computation of strongly compressible rotating flows. *J. Comput. Phys.* **38**, 335–356.

HARLOW, F. H. & MEIXNER, B. D. 1961 Motion of a viscous compressible gas adjacent to a sliding plate. *Phys. Fluids* **4**, 1202–1206.

HOWARTH, L. 1951 Some aspects of Rayleigh's problem for a compressible fluid. *Q. J. Mech. Appl. Maths* **4**, 157–169.

HYUN, J. M. 1983 Axisymmetric flows in spin-up from rest of a stratified fluid in a cylinder. *Geophys. Astrophys. Fluid Dyn.* **23**, 127–141.

HYUN, J. M., LESLIE, F., FOWLIS, W. W. & WARN-VARNAS, A. 1983 Numerical solutions for spin-up from rest in a cylinder. *J. Fluid Mech.* **127**, 263–281.

HYUN, J. M. & PARK, J. S. 1989 Some aspects of compressible Rayleigh's problem in a rotating cylinder. *J. Phys. Soc. Japan* **58**, 159–166.

KITCHEN, C. W. 1980 Navier–Stokes solutions for spin-up in a filled cylinder. *AIAA J.* **18**, 929–934.

PARK, J. S. & HYUN, J. M. 1989 Transient adjustment of a gas contained in a rapidly-rotating infinite cylinder. *J. Phys. Soc. Japan* **58**, 3949–3959.

PARK, J. K. & HYUN, J. M. 1990 Numerical solution for thermally driven compressible flows in a rapidly-rotating cylinder. *Fluid Dyn. Res.* **6**, 139–153.

PARK, J. K. & HYUN, J. M. 1991 Effects of thermal boundary conditions on rapidly-rotating gas flow. *Fluid Dyn. Res.* **7**, 119–129.

SAKURAI, T. & MATSUDA, T. 1974 Gasdynamics of a centrifugal machine. *J. Fluid Mech.* **62**, 727–736.

STEWARTSON, K. 1955 On the motion of a flat plate at high speed in a viscous compressible fluid. *Proc. Camb. Phil. Soc.* **51**, 202–219.

UNGARISH, M. & ISRAELI, M. 1985 Axisymmetric compressible flow in a rotating cylinder with axial convection. *J. Fluid Mech.* **154**, 121–144.

WARN-VARNAS, A., FOWLIS, W. W., PIACSEK, S. & LEE, S. M. 1978 Numerical solutions and laser-Doppler measurements of spin-up. *J. Fluid Mech.* **85**, 609–639.

WATKINS, W. B. & HUSSEY, R. G. 1973 Spin-up from rest: limitations of the Wedemeyer model. *Phys. Fluids* **16**, 1530–1531.

WATKINS, W. B. & HUSSEY, R. G. 1977 Spin-up from rest in a cylinder. *Phys. Fluids* **20**, 1596–1604.

WEDEMEYER, E. H. 1964 The unsteady flow within a spinning cylinder. *J. Fluid Mech.* **20**, 383–399.

WEIDMAN, P. D. 1976 On the spin-up and spin-down of a rotating fluid. *J. Fluid Mech.* **77**, 685–708.